Waveform inversion for microseismic velocity analysis and event location in VTI media*

Oscar Jarillo Michel and Ilya Tsvankin
Center for Wave Phenomena, Colorado School of Mines

ABSTRACT

Waveform inversion (WI), which has been extensively used in reflection seismology, could provide improved velocity models and event locations for microseismic surveys. Here, we develop an elastic WI algorithm for anisotropic media designed to estimate the 2D velocity field along with the source parameters (location, origin time, and moment tensor) from microseismic data. The gradient of the objective function is obtained with the adjoint-state method, which requires just two modeling simulations at each iteration. In the current implementation the source coordinates and velocity parameters are estimated sequentially at each stage of the inversion to minimize trade-offs and improve the convergence. Synthetic examples illustrate the accuracy of the inversion for layered VTI (transversely isotropic with a vertical symmetry axis) media, as well as the sensitivity of the velocity-analysis results to noise, the length of the receiver array, errors in the initial model, and variability in the moment tensor of the recorded events.

1 INTRODUCTION

Waveform inversion (Lailly, 1983; Tarantola, 1984; Virieux and Operto, 2009) is a nonlinear optimization method that has achieved significant success in building high-resolution velocity models from seismic data. The power of this approach lies in the opportunity to employ the phase and amplitude information contained in seismic records.

A crucial factor in making WI feasible is computation of the gradient of the objective function using the adjoint-state method (Lions, 1972; Plessix, 2006; Fichtner, 2006, 2009), which is more efficient than the more traditional approach based on the Fréchet derivatives. The adjoint-state method makes it possible to estimate the gradient for different classes of parameters using the same modeling simulations. Closed-form expressions for the gradient can be obtained from the adjoint wavefield simulated by the back-projection of the data residuals computed for a trial model. The cost of implementing the adjoint-state method is proportional to the number of sources but does not depend on the number of receivers (e.g., Tape et al., 2007).

Whereas most existing waveform-inversion algorithms designed for velocity analysis are acoustic, WI has been extended to multicomponent data from elastic isotropic (Mora, 1987; Prieux et al., 2013; Vigh et al., 2014) and anisotropic media (Lee et al., 2010; Kamath and Tsvankin, 2013, 2016). Although these methods are devised for reflected and diving waves acquired at the surface, elastic anisotropic WI is an attractive technique for microseismic data, which are typically recorded with multicomponent geophones. For microseismic studies, source locations and velocity structure can be estimated simultaneously using anisotropic traveltime inversion (Grechka and Yaskevich, 2014). This approach helps avoid location errors resulting from an incorrect velocity model and produces improved estimates of the medium parameters. Even more accurate event locations and higher-resolution velocity models can be expected from WI because it operates with entire waveforms and could include multiples, scattered waves, etc. in addition to the direct arrivals.

In earthquake seismology, WI has been used to estimate (although not simultaneously) the isotropic velocity structure and the source location and mechanism (Tape et al., 2007; Fichtner, 2009; Kim et al., 2011). Jarillo Michel and Tsvankin (2014, hereafter referred to as Paper I) extend the approach of Kim et al. (2011) to compute the gradient of the WI objective function in anisotropic media with respect to the microseismic source location $\mathbf{x}^s$, origin time t_0, and moment tensor $\mathbf{M}$. The gradient calculation is implemented for microseismic borehole data from 2D VTI models. Paper I also shows that the adjoint wavefield can be used to identify sources missing in the trial model. Jarillo Michel and Tsvankin (2015, Paper II) use the gradient expressions from Paper I to iteratively minimize the WI objective function and estimate the parameters $\mathbf{x}^s$, t_0, and $\mathbf{M}$ from 2D multicomponent microseismic data. The nondimensionalization technique (Kim et al., 2011) is used to update all model parameters simultaneously. Paper II presents synthetic tests for a vertical receiver array in VTI media to

*This paper has been accepted for publication in Geophysics. It represents a significantly revised and expanded version of Research Report CWP-860.

prove that all source parameters can be recovered if the velocity model is sufficiently accurate.

An important issue for waveform inversion is the choice of parameterization, especially if the model is anisotropic. Parameterizations proposed for WI in acoustic VTI media include different combinations of the P-wave vertical (V_{P0}), NMO ($V_{\rm nmo} = V_{P0}\sqrt{1+2\delta}$), and horizontal ($V_{\rm hor} = V_{P0}\sqrt{1+2\epsilon}$) velocities and the anisotropy coefficients ϵ, δ, and $\eta = (\epsilon-\delta)/(1+2\delta)$. Alkhalifah and Plessix (2014) demonstrate that a parameter set consisting of the horizontal velocity $V_{\rm hor}$ and the coefficients ϵ and η reduces trade-offs when diving waves dominate the updates (i.e., for long-offset data). Application of elastic WI to P- and SV-waves requires including an additional VTI parameter that influences S-wave propagation, such as the shear-wave vertical velocity V_{S0} (Kamath et al., 2016).

Here, we extend the inversion for the source parameters presented in Paper II to incorporate anisotropic velocity analysis, which involves processing of multiple microseismic events. To mitigate parameter trade-offs, the iterative WI algorithm estimates the source coordinates and VTI velocity field in a sequential fashion. The model is parameterized by $V_{\rm hor}$, V_{S0}, η, and ϵ following Alkhalifah and Plessix (2014) and Kamath et al. (2016), which allows us to take advantage of near-horizontal wave propagation in downhole arrays.

First, we review the WI methodology including the gradient computation for both the source and velocity parameters. Then, assuming the source parameters to be known, we invert synthetic data from horizontally layered VTI media recorded by a vertical receiver array for the interval values of $V_{\rm hor}$, V_{S0}, η, and ϵ. The inversion for the velocity model is also tested on data contaminated by band-limited random noise, recorded by a shorter receiver array, and excited by sources with a range of fault orientations. Finally, we implement sequential inversion for both the source coordinates and medium parameters and apply it to multiazimuth borehole data from laterally homogeneous VTI media. The results illustrate the sensitivity of the inversion to the accuracy of the initial model and confirm the improvements in event location and velocity estimation provided by waveform inversion.

2 WAVEFORM-INVERSION METHODOLOGY

The algorithm operates with the elastic wave equation for a point source in a heterogeneous anisotropic medium:

$$\rho\,\frac{\partial^2 u_i}{\partial t^2} - \frac{\partial}{\partial x_j}\left(c_{ijkl}\,\frac{\partial u_k}{\partial x_l}\right) = -\,M_{ij}\frac{\partial[\delta(\mathbf{x}-\mathbf{x}^s)]}{\partial x_j}\,S(t)\;, \tag{1}$$

where $\mathbf{u}(\mathbf{x},t)$ is the displacement field, t is time, c_{ijkl} is the stiffness tensor ($i,j,k,l = 1,2,3$), $\rho\,(\mathbf{x})$ is density, $\mathbf{M}$ is the seismic moment tensor, $\mathbf{x}^s$ is the source location, $S(t)$ is the source time function, and $\delta(\mathbf{x}-\mathbf{x}^s)$ is the spatial δ-function. Summation over repeated indices is implied. Here, we employ 2D finite-difference modeling to solve equation 1 for heterogeneous VTI media.

The data residuals are measured by the ℓ_2-norm objective function $\mathcal{F}$, which is commonly used in WI:

$$\mathcal{F}(\mathbf{m}) = \frac{1}{2}\sum_{n=1}^{N}\left\|\mathbf{d}_{\rm pre}(\mathbf{m}) - \mathbf{d}_{\rm obs}\right\|^2\;, \tag{2}$$

where $\mathbf{d}_{\rm obs}$ is the observed displacement and $\mathbf{d}_{\rm pre}(\mathbf{m})$ is the displacement simulated for the trial model $\mathbf{m}$. The wavefield excited by each microseismic event is recorded by N receivers positioned at $\mathbf{x}^{r_n}$ ($n = 1,2,...,N$); the function $\mathcal{F}$ also involves summation over all available sources.

2.1 Gradient for source parameters

Computation of the gradient of the objective function with respect to the source coordinates x_1^s and x_3^s, origin time t_0, and moment-tensor elements M_{ij} is discussed in Paper I. P- and SV-waves propagating in the $[x_1,\,x_3]$-plane depend only on the components M_{11}, M_{13}, and M_{33}, which can be represented for dip-slip dislocation sources as a function of the fault dip angle θ.

The derivatives of the objective function with respect to the source parameters can be found from the adjoint-state method as (Paper I):

$$\frac{\partial\mathcal{F}}{\partial x_i^s} = \int_0^T \frac{\partial[\mathbf{M}:\boldsymbol{\epsilon}^\dagger(\mathbf{x}^{ts},t)]}{\partial x_i}\bigg|_{\mathbf{x^{ts}}} S(T-t)\,{\rm d}t\;, \tag{3}$$

$$\frac{\partial\mathcal{F}}{\partial t_0} = \int_0^T \mathbf{M}:\boldsymbol{\epsilon}^\dagger(\mathbf{x}^{ts},t)\,\frac{\partial S(T-t)}{\partial t}\,{\rm d}t\;, \tag{4}$$

and

$$\frac{\partial\mathcal{F}}{\partial M_{ij}} = \int_0^T \epsilon_{ij}^\dagger(\mathbf{x}^{ts},t)\,S(T-t)\,{\rm d}t\;, \tag{5}$$

where $\mathbf{x}^{ts}$ is the trial source location, T is the recording time, and $\boldsymbol{\epsilon}^\dagger$ is the adjoint strain tensor. The derivatives in equations 3 – 5 are needed only at the trial source position (i.e., where the source parameters should be updated).

In Paper II we perform simultaneous inversion for $\mathbf{x}^s$, t_0, and $\mathbf{M}$ for 2D VTI media employing the nondimensionalization approach suggested by Kim et al. (2011) and assuming the velocity model to be known. An appropriate scaling of the gradient ensures that the derivatives of $\mathcal{F}$ with respect to all model parameters have the same order of magnitude.

2.2 Gradient for medium parameters

Reliable estimation of event locations and source mechanisms in microseismic monitoring requires an accurate velocity model. The WI algorithm proposed here is designed to recover the anisotropic velocity model along with the source parameters under the assumption of VTI symmetry. Hence, the objective function combines the data residuals for all available

sources. The derivatives of the objective function $\mathcal{F}$ with respect to the stiffness coefficients c_{ijkl} can be obtained using the adjoint-state method (Liu and Tromp, 2006; Kamath and Tsvankin, 2016):

$$\frac{\partial \mathcal{F}}{\partial c_{ijkl}} = -\int_0^T \frac{\partial \mathrm{u}_i}{\partial x_j}\frac{\partial \psi_k}{\partial x_l}\ , \tag{6}$$

where $\mathbf{u}$ and $\boldsymbol{\psi}$ are the forward and adjoint displacement fields, respectively. The gradient for the chosen model parameters m_n can be found from the chain rule:

$$\frac{\partial \mathcal{F}}{\partial m_n} = \sum_{ijkl}\frac{\partial \mathcal{F}}{\partial c_{ijkl}}\frac{\partial c_{ijkl}}{\partial m_n}\ . \tag{7}$$

Therefore, the gradient for both the source (equations 3 – 5) and velocity parameters can be computed from the same forward and adjoint wavefields generated by two modeling simulations. This means that velocity analysis is performed at little extra cost but, of course, it may introduce additional parameter trade-offs.

Following Alkhalifah and Plessix (2014) and Kamath et al. (2016), we parameterize the medium by $(V_{\mathrm{hor}}/V_{\mathrm{hor}_i})^2$, $(V_{S0}/V_{S0_i})^2$, $(1+2\eta)$, and $(1+2\epsilon)$; the subscript i stands for the initial value. The velocities in this parameterization are normalized by the squares of their respective initial values, which makes all parameters dimensionless and reduces them to the same order of magnitude. The explicit expressions for the derivatives of the objective function with respect to these parameters are given in Appendix A.

2.3 Implementation

We update the model with the $l-$BFGS method (Byrd et al., 1995), which approximates the inverse of the full Hessian matrix using the gradient of the objective function computed at previous iterations. This method generally produces better convergence than the more conventional steepest-descent and nonlinear conjugate-gradient techniques.

In the current implementation, the source and medium parameters are estimated separately in a sequential fashion, which helps mitigate parameter trade-offs that would result from simultaneous inversion. First, the inversion algorithm iteratively estimates the source coordinates of all available events using the initial velocity model. Then the inverted source locations are employed to iteratively update the velocity model. The refined velocity model is used to further update the source coordinates and the process continues until the objective function flattens out. Alternatively, if the initial source locations are believed to be sufficiently accurate, the sequential inversion can start with velocity updating followed by source-parameter estimation. The origin times and source moment tensors can be estimated as well, but currently they are fixed at the actual values to mitigate parameter trade-offs.

Although the examples shown below and in Paper II are for 2D models, this WI algorithm is applicable to 3D data from layer-cake VTI media. Indeed, if the source-receiver azimuth can be estimated from the polarization of the direct P-wave, the in-plane horizontal displacement component employed in our methodology can be computed by a simple receiver rotation. Because the medium is laterally homogeneous, this rotation "moves" the wavefields from all events to the same vertical plane. Then the rotated wavefields from sources at different azimuths can be simultaneously inverted using the proposed 2D WI algorithm.

3 SYNTHETIC EXAMPLES

3.1 Inversion for VTI parameters

First, we estimate the interval parameters of the horizontally layered (1D) VTI model from Figure 1 using the vertical and horizontal displacement components recorded by a vertical receiver array. Although the medium is laterally homogeneous, we apply WI using a general 2D gridded model (grid spacing is 3 m) because the algorithm is designed to handle both vertical and lateral heterogeneity. The initial 1D model for all parameters is obtained by smoothing the actual fields in the vertical direction; also, each of the model parameters contains an additional perturbation in the middle layer (Figure 2).

For any WI algorithm, it is essential to have a starting model that generates synthetic data within a half-period of the observed data to avoid cycle skipping. Given the low frequency of the source wavelet used in this test and the relatively short distance between the sources and the receiver array, the initial model from Figure 2 complies with this requirement. The source parameters of all 10 generated microseismic events are assumed to be known and the inversion is performed without any smoothness constraints. The search is terminated after about 19 iterations when the objective function becomes sufficiently small (Figure 3).

The results of this test (Figure 4) benefit from the relatively wide aperture of the source-receiver directions (Figure 1). The 2D inversion result in Figure 5, however, shows some distortions (especially near the ends of the line) mainly caused by the small number of events and the uneven amplitude distribution along the generated wavefronts. As expected, the velocity V_{hor} in the employed parameterization is well-constrained for near-horizonal wave propagation in this test (Alkhalifah and Plessix, 2014). Because V_{S0} represents both the vertical and horizontal SV-wave velocity, it can also be accurately estimated in this geometry for the middle part of the section (Figure 6). Also, P-waves traveling at oblique directions with propagation angles approaching 45° help estimate the coefficient η. However, WI of P-waves for this parameterization is weakly sensitive to the parameter ϵ, unless near-vertical raypaths are available (Alkhalifah and Plessix, 2014). Our results show that SV-waves do not provide sufficient information to constrain that parameter either.

3.1.1 Influence of noise and length of receiver array

Next, we add random Gaussian noise (the signal-to-noise ratio is close to 12) in the frequency band of the signal to the ob-

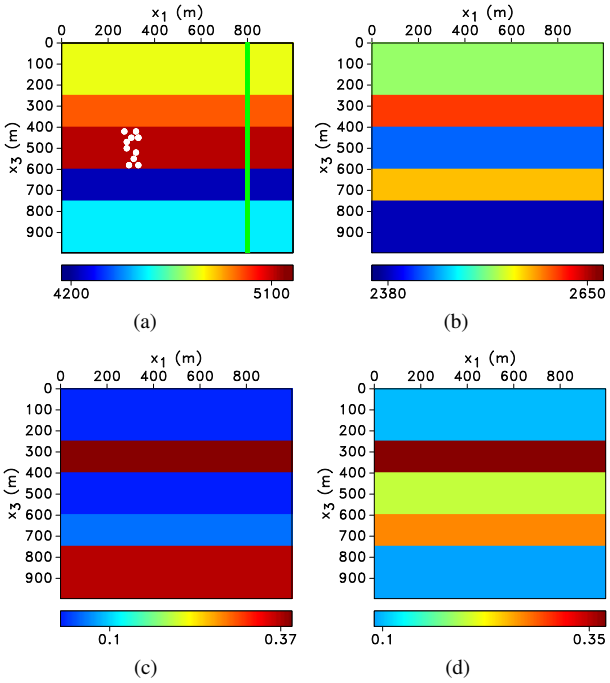

Figure 1. Sources (white dots) and receivers (green line) embedded in a layered VTI medium with the parameters (a) $V_{\rm hor}$, (b) V_{S0}, (c) η, and (d) ϵ (velocities are in $\rm m/s$). All 10 events represent dip-slip sources with the fault plane dipping at 30°. The central frequency of the source signal is 20 Hz.

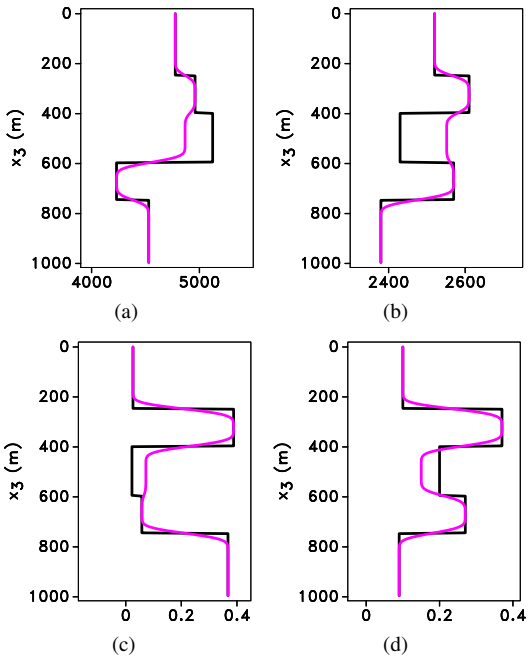

Figure 2. Actual (black) and initial (magenta) VTI parameters for the model in Figure 1: (a) $V_{\rm hor}$, (b) V_{S0}, (c) η, and (d) ϵ (velocities are in $\rm m/s$). There is a substantial distortion in the initial parameters in the middle layer.

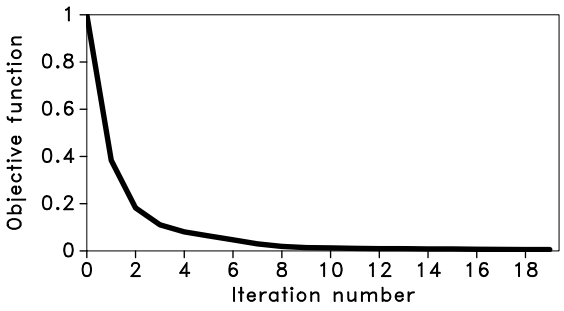

Figure 3. Change of the normalized objective function $\mathcal{F}(\mathbf{m})$ with iterations for the model in Figure 1.

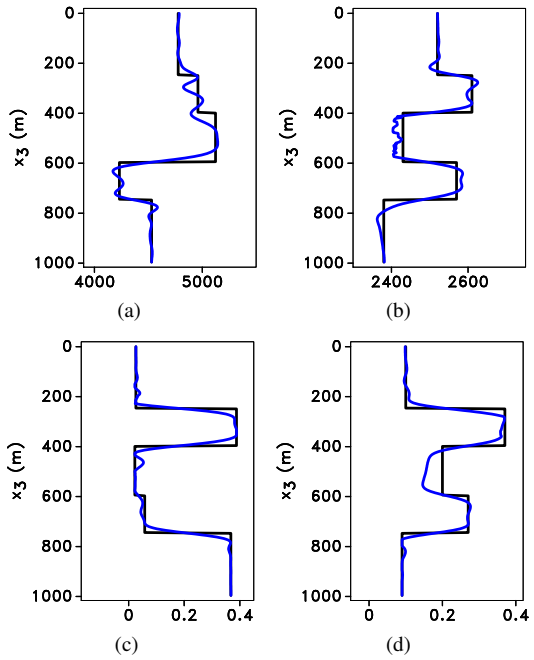

Figure 4. Actual (black) and inverted (blue) VTI parameters for the model in Figure 1: (a) $V_{\rm hor}$, (b) V_{S0}, (c) η, and (d) ϵ (velocities are in $\rm m/s$). The inversion is performed using the initial model from Figure 2. The profiles are plotted at $x_1 = 600\,\rm m$.

served displacements for the model in Figure 1 (Figure 7). As shown in Figure 8, the objective function cannot be reduced as much as for noise-free data. Still, despite the considerable magnitude of noise, the distortions in the inverted parameters for the middle part of the model are not significant (Figure 9). As expected, the errors are more pronounced in the layers near the top and bottom of the section, where the illumination is more sparse.

The previous tests were performed for a receiver array that covers the entire vertical extent of the section, which may not be realistic for field experiments. Therefore, we repeat the inversion using data recorded by a shorter vertical receiver array (Figure 10). The initial model is the same as the one used in the first test (Figure 2). Despite the reduced length of the ar-

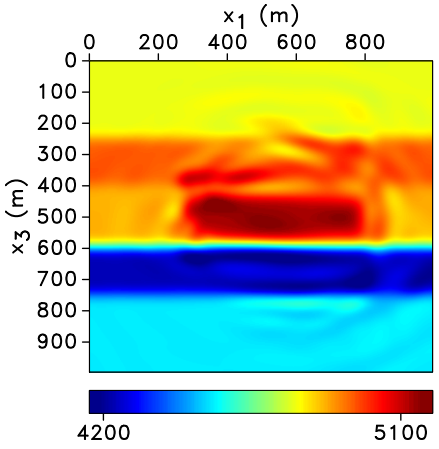

Figure 5. 2D field of the inverted velocity $V_{\rm hor}$ (in m/s).

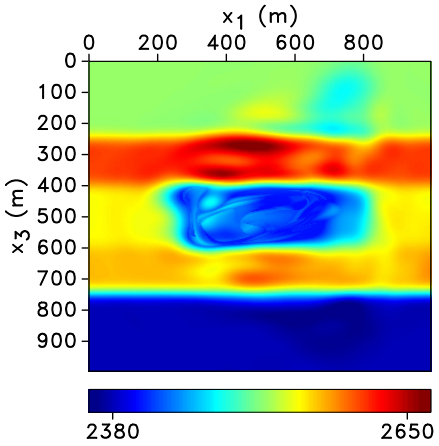

Figure 6. 2D field of the inverted velocity V_{S0} (in m/s).

ray, the inverted parameters remain close to the actual values (Figure 11). The only exception is a distortion in the velocity V_{S0} near the top of the model caused by insufficient illumination.

3.1.2 Test with different source orientations

In general, the source mechanisms (moment tensors) of the events in microseismic surveys may differ. To analyze the performance of the algorithm in such cases, we repeat the test for the model in Figure 1 but use faulting sources with a range of dip angles (from 15° to 60°). Although in this example we employ only dislocation-type sources (which are most common in microseismic studies), the algorithm can handle any other source types (i.e., an arbitrary moment tensor $\mathbf{M}$). Interestingly, the inversion results for all four parameters (Figure 12) are somewhat better than those for the same source orientation (Figure 4). Indeed, the presence of events with different fault orientations results in a more uniform wavefield coverage at the receivers because the low-amplitude wavefront segments

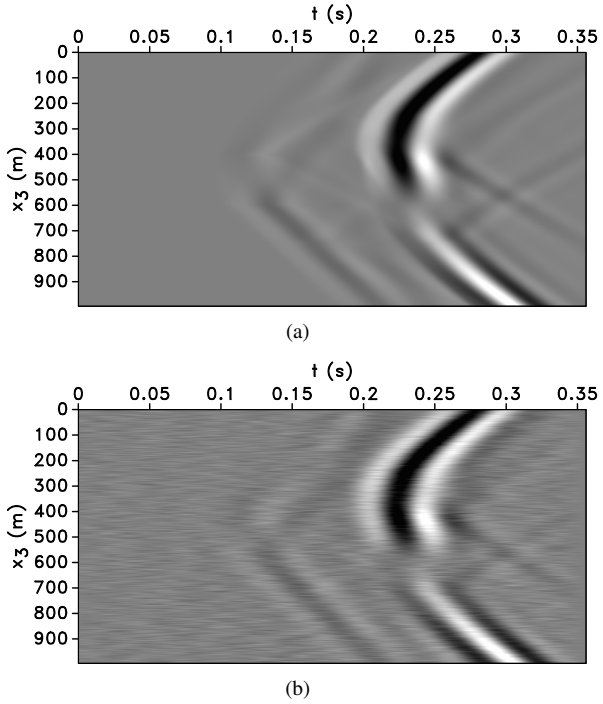

Figure 7. Observed vertical displacement (a) without and (b) with Gaussian noise for the source at $x_1 = 330\,\mathrm{m}$ and $x_3 = 450\,\mathrm{m}$ in the model from Figure 1. The noise has the same frequency band as the data and the signal-to-noise ratio is 11.9. The source (dip-slip fault with $\theta = 30^\circ$) produces strong amplitude variations along the P- and S- wavefronts near the horizontal plane.

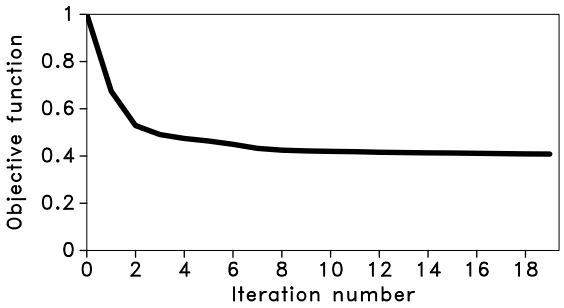

Figure 8. Change of the normalized objective function $\mathcal{F}(\mathbf{m})$ with iterations for the model in Figure 1. The observed data are contaminated by noise (Figure 7). The initial model is shown in Figure 2.

of the individual wavefields correspond to different propagation directions.

3.2 Sequential inversion for multiazimuth source array

The WI methodology discussed above is designed to estimate both the source and VTI parameters. We implement the inversion in a sequential fashion, where at each stage we iteratively estimate first the source coordinates and then the velocity model (or vice versa). We test this sequential inversion

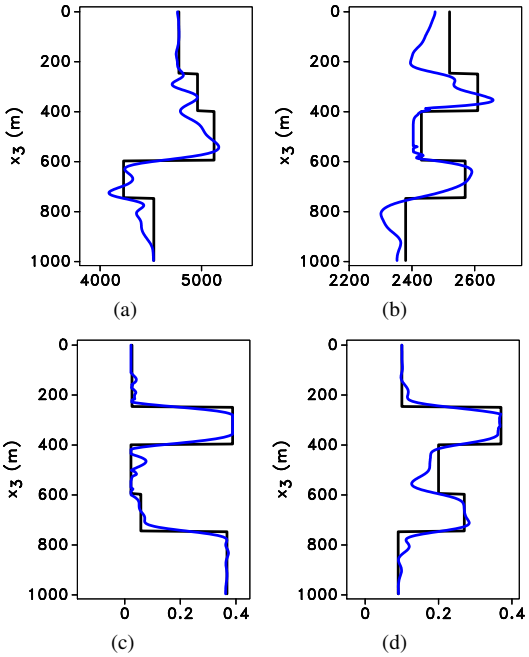

Figure 9. Actual (black) and inverted (blue) VTI parameters for the model in Figure 1: (a) $V_{\rm hor}$, (b) V_{S0}, (c) η, and (d) ϵ (velocities are in $\rm m/s$). The observed data are contaminated by noise (Figure 7). The profiles are plotted at $x_1 = 600\,\rm m$.

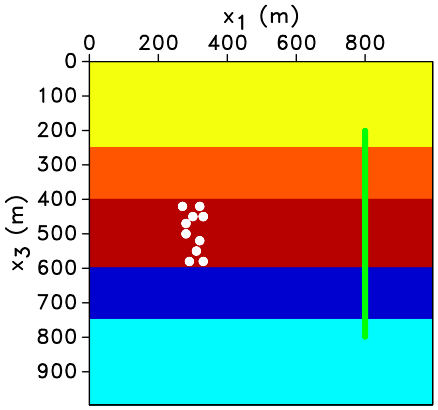

Figure 10. Sources (white dots) and a shorter array of receivers (green line) embedded in the layered VTI medium from Figure 1. All events represent dip-slip sources with the dip angle $\theta = 30°$. The central frequency of the source signal is 20 Hz.

for a multiazimuth source array embedded in the horizontally layered VTI model (Figure 13) under the assumption that the origin times and source mechanisms of the recorded events are known. Figure 14 shows the sources projected onto the same vertical plane of the model and the vertical receiver array. The initial source coordinates in the vertical plane (x_1^s and x_3^s) are distorted by ± 20 m, which might cause the inversion algorithm to get trapped in local minima, especially if the velocity

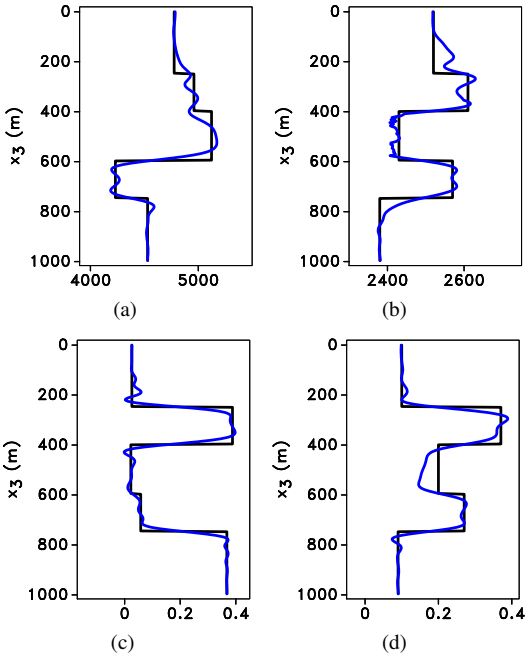

Figure 11. Actual (black) and inverted (blue) VTI parameters for the model in Figure 10 with a shorter receiver array: (a) $V_{\rm hor}$, (b) V_{S0}, (c) η, and (d) ϵ (velocities are in $\rm m/s$). The inversion is performed using the initial model from Figure 2. The profiles are plotted at $x_1 = 600\,\rm m$.

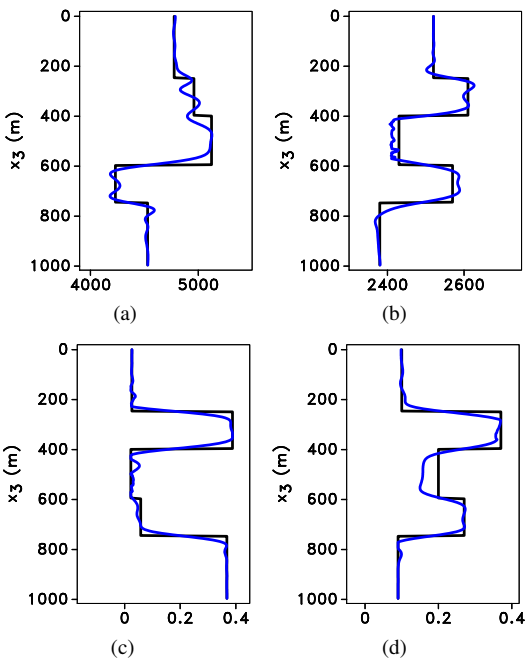

Figure 12. Actual (black) and inverted (blue) VTI parameters for the model in Figure 1 with different source orientations: (a) $V_{\rm hor}$, (b) V_{S0}, (c) η, and (d) ϵ (velocities are in $\rm m/s$). The dip angles of the dip-slip sources vary from $15°$ to $60°$. The inversion is performed using the initial model from Figure 2. The profiles are plotted at $x_1 = 600\,\rm m$.

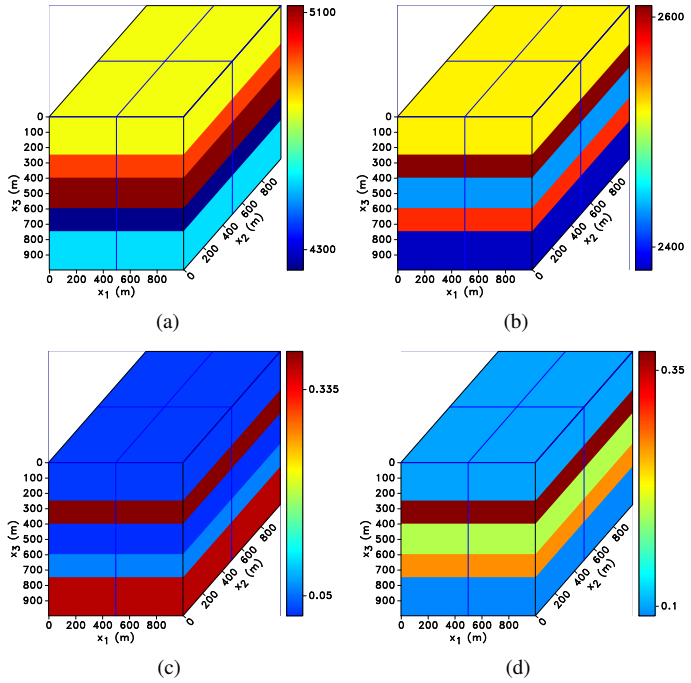

Figure 13. Horizontally layered VTI medium used to test the sequential inversion for a multiazimuth source array: (a) $V_{\rm hor}$, (b) V_{S0}, (c) η, and (d) ϵ (velocities are in $\rm m/s$).

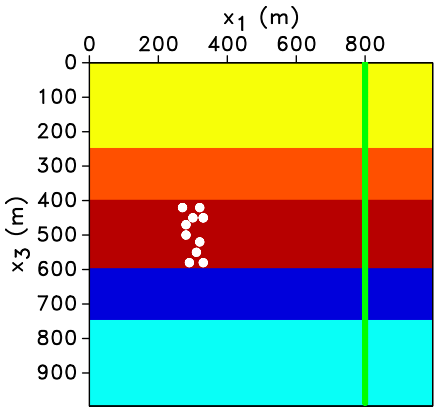

Figure 14. Vertical plane of the VTI model in Figure 13 that contains the receiver array (green line). White dots are the projections of the sources which are located at different azimuths (within the $\pm 20^\circ$ range). All events represent dip-slip sources with the dip angle $\theta = 30^\circ$. The central frequency of the source signal is 20 Hz.

field is also inaccurate. In this test, however, the initial velocity model in Figure 15 does not produce cycle skipping.

The azimuths of all events (assumed to be estimated from P-wave polarization) are used to rotate the horizontal displacements into the radial (in-plane) and transverse components. Then the radial and vertical displacements are inverted by our 2D algorithm. The inversion starts with iterative refinement of event locations using the initial velocity model. Then iterative

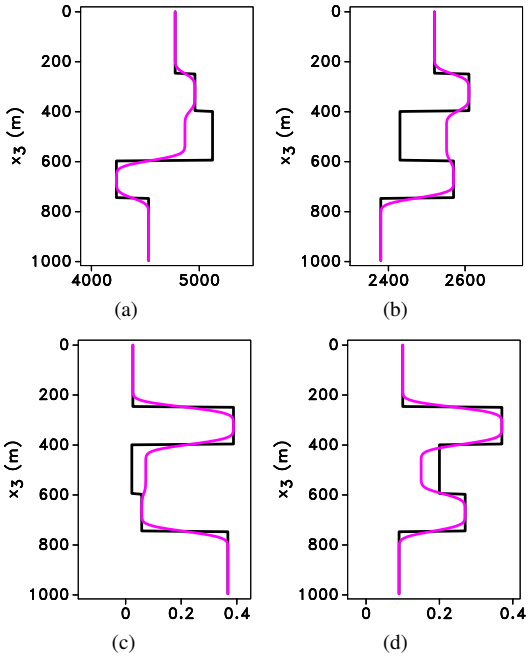

Figure 15. Actual (black) and initial (magenta) VTI parameters for the model in Figure 14: (a) $V_{\rm hor}$, (b) V_{S0}, (c) η, and (d) ϵ (velocities are in $\rm m/s$). There is a distortion in the initial parameters in the middle layer.

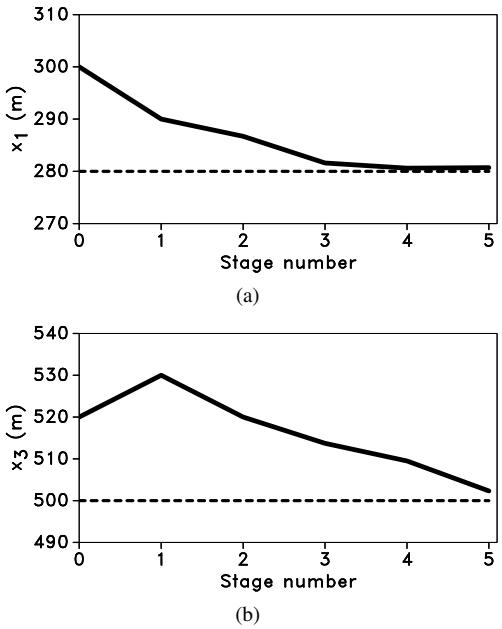

Figure 16. Change of the source coordinates (a) $x_1^{\rm s}$ and (b) $x_3^{\rm s}$ with inversion stages for one of the sources in the model from Figure 14. The actual values are indicated by the horizontal dashed lines. Similar results were obtained for all other sources.

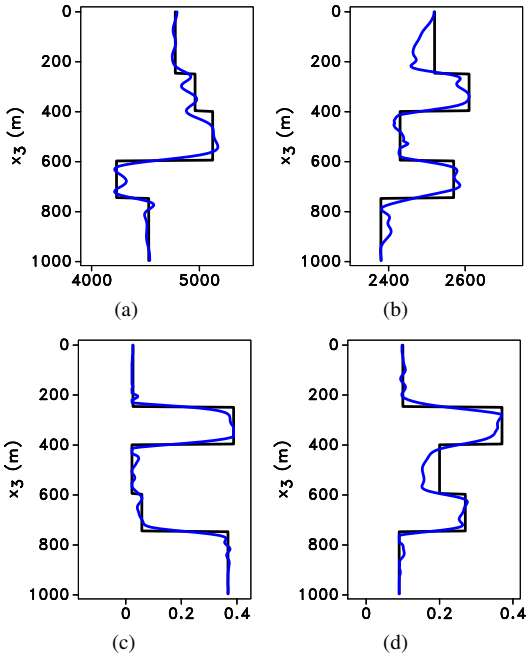

Figure 17. Actual (black) and inverted (blue) VTI parameters for the model in Figure 14 after the fifth stage of inversion: (a) $V_{\rm hor}$, (b) V_{S0}, (c) η, and (d) ϵ (velocities are in $\rm m/s$). The profiles are plotted at $x_1 = 600\,\rm m$.

inversion for the interval VTI parameters is performed with the updated source coordinates. This process, carried out five times (i.e., there are five inversion stages), produces improved estimates of the source coordinates (Figure 16) and velocity parameters (Figure 17). There are some distortions in the inverted parameters mainly close to the edges of the model due to sparse coverage, limited number of events, and the trade-off between the source coordinates and velocity parameters.

4 CONCLUSIONS

We extended the elastic waveform-inversion algorithm presented in our previous publications to velocity model-building from microseismic data. The gradient of the objective function with respect to the source and medium parameters is obtained with the adjoint-state method for 2D gridded VTI media. To mitigate nonuniqueness, the source coordinates and velocity parameters are estimated separately in a sequential fashion. The VTI model is described by the parameters $V_{\rm hor}$, V_{S0}, η, and ϵ; this parameter set was shown to be beneficial for minimizing trade-offs when waves travel predominantly near the horizontal direction. Although the current algorithm is designed in 2D, it is fully applicable to downhole microseismic data generated by a multiazimuth array of sources in layer-cake VTI media.

First, the algorithm was applied to velocity analysis of P- and SV-waves recorded by a vertical receiver array embedded in a layered VTI medium. With the source parameters fixed at the actual values and the receivers covering the entire vertical extent of the model, WI accurately recovered all four interval VTI parameters. The distortions in the inverted parameters were relatively small and limited mostly to the edges of the model. The algorithm can tolerate errors on the order of 5% in the initial values of $V_{\rm hor}$, V_{S0}, and η because these parameters are well-resolved for near-horizontal P-wave propagation. In contrast, the initial ϵ-field should be close to the actual model, unless near-vertical raypaths are available. The inversion remains sufficiently accurate for a shorter receiver array, variable source (fault) orientation, and in the presence of moderate band-limited random noise. Deviations from the actual model are observed primarily near the top and bottom of the section due to insufficient illumination.

The last test demonstrated the feasibility of sequential inversion for the source coordinates and velocity parameters of layer-cake VTI media using multicomponent data from a multiazimuth cloud of sources. Inversion for this model can be performed by our 2D algorithm after rotating the recorded displacements into the radial and transverse components. The objective function was sufficiently reduced after five stages of the inversion, where each stage included iterative updating of the source coordinates followed by iterative velocity estimation.

In a previous paper, we showed that the algorithm can also be used to invert for the source mechanisms but full reconstruction of the moment tensor from microseismic data has to be performed in 3D and typically requires taking azimuthal anisotropy into account. Extension of the algorithm to azimuthally anisotropic 3D models is a topic of ongoing research.

5 ACKNOWLEDGMENTS

We are grateful to Vladimir Grechka (Marathon Oil) for his insights and feedback regarding various aspects of this research. This work was supported by the Consortium Project on Seismic Inverse Methods for Complex Structures at the Center for Wave Phenomena (CWP).

REFERENCES

Alkhalifah, T., and R. Plessix, 2014, A recipe for practical full-waveform inversion in anisotropic media: An analytical parameter resolution study: Geophysics, **79**, no. 3, R91–R101.

Byrd, R. H., P. Lu, J. Nocedal, and C. Zhu, 1995, A limited memory algorithm for bound constrained optimization: SIAM Journal on Scientific Computing, **16**, no. 5, 1190–1208.

Fichtner, A., 2006, The adjoint method in seismology: I. Theory: Physics of the Earth and Planetary Interiors, **157**, no. 12, 86–104.

———, 2009, Full seismic waveform inversion for structural and source parameters: PhD thesis, Ludwig-Maximilians-Universität München.

Grechka, V., and S. Yaskevich, 2014, Azimuthal anisotropy in microseismic monitoring: A Bakken case study: Geophysics, **79**, no. 1, KS1–KS12.

Jarillo Michel, O., and I. Tsvankin, 2014, Gradient calculation for waveform inversion of microseismic data in VTI media: Journal of Seismic Exploration, **23**, no. 3, 201–217.

———, 2015, Estimation of microseismic source parameters by 2D anisotropic waveform inversion: Journal of Seismic Exploration, **24**, no. 5, 379–400.

Kamath, N., and I. Tsvankin, 2013, Full-waveform inversion of multicomponent data for horizontally layered VTI media: Geophysics, **78**, no. 5, WC113–WC121.

———, 2016, Elastic full-waveform inversion for VTI media: Methodology and sensitivity analysis: Geophysics, **81**, no. 2, C53–C68.

Kamath, N., I. Tsvankin, and E. Díaz, 2016, Elastic FWI for VTI media: A synthetic parameterization study: CWP Project Review Report.

Kim, Y., Q. Liu, and J. Tromp, 2011, Adjoint centroid-moment tensor inversions: Geophysical Journal International, **186**, no. 1, 264–278.

Lailly, P., 1983, The seismic inverse problem as a sequence of before stack migrations: Bednar, J. B., Redner, R., Robinson, E., and Weglein, A., Eds., Conference on Inverse Scattering: Theory and Application, Soc. Industr. Appl. Math., 206–220.

Lee, H.-Y., J. M. Koo, D.-J. Min, B.-D. Kwon, and H. S. Yoo, 2010, Frequency-domain elastic full waveform inversion for VTI media: Geophysical Journal International, **183**, no. 2, 884–904.

Lions, J., 1972, Nonhomogeneous boundary value problems and applications: Springer Verlag, Berlin.

Liu, Q., and J. Tromp, 2006, Finite-frequency kernels based on adjoint methods: Bulletin of the Seismological Society of America, **96**, no. 6, 2383–2397.

Mora, P., 1987, Nonlinear two-dimensional elastic inversion of multioffset seismic data: Geophysics, **52**, no. 9, 1211–1228.

Plessix, R.-E., 2006, A review of the adjoint-state method for computing the gradient of a functional with geophysical applications: Geophysical Journal International, **167**, no. 2, 495–503.

Prieux, V., R. Brossier, S. Operto, and J. Virieux, 2013, Multiparameter full waveform inversion of multicomponent ocean-bottom-cable data from the Valhall field. Part 2: imaging compressive-wave and shear-wave velocities: Geophysical Journal International, **194**, no. 3, 1665.

Tape, C., Q. Liu, and J. Tromp, 2007, Finite-frequency tomography using adjoint methods - Methodology and examples using membrane surface waves: Geophysical Journal International, **168**, no. 3, 1105–1129.

Tarantola, A., 1984, Inversion of seismic reflection data in the acoustic approximation: Geophysics, **49**, no. 8, 1259–1266.

Vigh, D., K. Jiao, D. Watts, and D. Sun, 2014, Elastic full-waveform inversion application using multicomponent measurements of seismic data collection: Geophysics, **79**, no. 2, R63–R77.

Virieux, J., and S. Operto, 2009, An overview of full-waveform inversion in exploration geophysics: Geophysics, **74**, no. 6, WCC1–WCC26.

APPENDIX A: WI GRADIENT FOR THE VTI PARAMETERS

Following Kamath et al. (2016), we describe the elastic VTI model by four parameters:

$$m_1 = \left(V_{\rm hor}/V_{{\rm hor}_i}\right)^2 , \tag{A1}$$

$$m_2 = \left(V_{S0}/V_{S0_i}\right)^2 , \tag{A2}$$

$$m_3 = 1 + 2\eta , \tag{A3}$$

$$m_4 = 1 + 2\epsilon . \tag{A4}$$

Applying the chain rule to equation 7, the derivatives of the objective function (equation 2) for this parameterization are obtained as:

$$\frac{\partial \mathcal{F}}{\partial m_1} = -\rho\, V_{{\rm hor},i}^2 \int_0^T \left[\frac{\partial \psi_1}{\partial x_1}\frac{\partial u_1}{\partial x_1} + \frac{1}{1+2\epsilon}\frac{\partial \psi_3}{\partial x_3}\frac{\partial u_3}{\partial x_3} \right.$$

$$\left. + \frac{1}{2}\left(\frac{f}{1+2\epsilon} + \frac{1}{f(1+2\eta)}\right)\left(\frac{\partial \psi_3}{\partial x_3}\frac{\partial u_1}{\partial x_1} + \frac{\partial \psi_1}{\partial x_1}\frac{\partial u_3}{\partial x_3}\right)\right] dt, \tag{A5}$$

$$\frac{\partial \mathcal{F}}{\partial m_2} = -\rho\, V_{S0,i}^2 \int_0^T \left[\left(\frac{\partial \psi_1}{\partial x_3} + \frac{\partial \psi_3}{\partial x_1}\right)\left(\frac{\partial u_1}{\partial x_3} + \frac{\partial u_3}{\partial x_1}\right) \right.$$

$$\left. - \left(\frac{f}{2} + \frac{1}{2f} + 1\right)\left(\frac{\partial \psi_3}{\partial x_3}\frac{\partial u_1}{\partial x_1} + \frac{\partial \psi_1}{\partial x_1}\frac{\partial u_3}{\partial x_3}\right)\right] dt, \tag{A6}$$

$$\frac{\partial \mathcal{F}}{\partial m_3} = \frac{\rho\, V_{\rm hor}^2}{2f(1+2\eta)^2} \int_0^T \left(\frac{\partial \psi_3}{\partial x_3}\frac{\partial u_1}{\partial x_1} + \frac{\partial \psi_1}{\partial x_1}\frac{\partial u_3}{\partial x_3}\right) dt, \tag{A7}$$

$$\frac{\partial \mathcal{F}}{\partial m_4} = \frac{\rho\, V_{\rm hor}^2}{(1+2\epsilon)^2} \int_0^T \left[\frac{\partial \psi_3}{\partial x_3}\frac{\partial u_3}{\partial x_3} + \frac{f}{2}\left(\frac{\partial \psi_3}{\partial x_3}\frac{\partial u_1}{\partial x_1} + \frac{\partial \psi_1}{\partial x_1}\frac{\partial u_3}{\partial x_3}\right)\right] dt, \tag{A8}$$

where

$$f \equiv \sqrt{\frac{V_{\rm nmo}^2 - V_{S0}^2}{V_{P0}^2 - V_{S0}^2}} ; \tag{A9}$$

$\mathbf{u}$ and $\boldsymbol{\psi}$ are the forward and adjoint displacement fields, respectively.